Experimental and numerical analysis of foundation pilings partially embedded in rock

Análise experimental e numérica de estacas-raiz parcialmente embutidas em rocha

Jean Rodrigo Garcia
Unicamp, Campinas, Brazil.
eng.garcia@gmail.com

Paulo José Rocha de Albuquerque
Unicamp, Campinas, Brazil.
pjra@fec.unicamp.br

Rodrigo Álvares de Araújo Melo
Unicamp, Campinas, Brazil.
rodrigo.melo@mendesjunior.com.br

Resumo

Analisa-se o comportamento de quatro estacas-raiz (ϕ=0,41m) executadas na cidade de Foz do Iguaçu/PR, as quais foram submetidas a provas de carga com carregamento lento. Os resultados foram confrontados com aqueles obtidos por meio de modelagem numérica tridimensional pelo método dos elementos finitos, o qual permite simular o comportamento elásto-plástico do solo. O subsolo local apresenta variada estratigrafia, composto por uma camada superficial de solo residual, seguida por alteração de rocha e rocha sã em poucos metros de profundidade. Os parâmetros geotécnicos do maciço foram determinados por meio de correlações obtidas a partir de ensaios de campo, estimando-se os valores de coesão, ângulo de atrito, módulo de deformabilidade e resistência à compressão uniaxial das diferentes camadas do subsolo. As provas de cargas foram interrompidas quando alcançaram 3000 kN, apresentando deslocamentos inferiores a 5mm na carga de trabalho (1500 kN). Verificou-se que as estacas trabalharam por atrito lateral com tensões médias da ordem de 70 kPa, para o trecho superficial (solo residual), e superiores a 150 kPa, nos trechos em alteração de rocha. Os parâmetros geotécnicos estimados forneceram valores que se adequaram perfeitamente às análises numéricas. Nesse sentido, pôde-se verificar, através das análises realizadas e pelo modelo de transferência de carga, que seus comprimentos poderiam ser reduzidos, possibilitando otimizar o projeto geotécnico.

Palavras-chave: Estaca-raiz, embutimento em rocha, prova de carga, análise numérica tridimensional.

Abstract

The behaviours of four foundation pilings (ϕ=0.41 m) constructed in Foz do Iguaçu, Paraná (PR), Brazil and subjected to slow loading tests were analysed. The results were compared with results from three-dimensional numerical modelling using the finite element method, which facilitates simulation of the elasto-plastic behaviour of soil. The local subsoil comprises varied stratigraphies; it is composed of a residual soil surface layer followed by weathered rock and bedrock, which are a few meters deep. The massif geotechnical parameters were determined through correlations obtained from field tests, whereby the values for cohesion, angle of friction, modulus of deformability and uniaxial compressive strength in the different subsoil layers were estimated. The load tests were interrupted at 3000 kN and displaced by less than 5 mm in the working load (1500 kN). The pilings were subjected to lateral friction work

with an average stress of approximately 70 kPa for the surface portion (residual soil) and greater than 150 kPa for the weathered rock portions. The estimated geotechnical parameters provided values that were an exact match with the numerical analyses. Thus, given the analyses and load transfer method, the piling lengths can be reduced, which will facilitate the optimisation of the geotechnical design.

Keywords: *Foundation piling, rock embedding, load test, three-dimensional numerical analysis.*

1. Introduction

The subsoil stratigraphic composition can aid in elucidating the behaviour of a foundation element that is subject to a specific force. However, delimitation may be uncertain among the various layers that comprise a massif, and geotechnical parameters for such materials will aid in correctly determining the beginning and end of a layer, especially for soil followed by a rocky massif.

According to Rocha (1977), uniaxial strength and cohesion are the most appropriate characteristics for establishing a boundary between soils and rocks. According to this author, the angle of friction is an ineffective parameter for distinguishing between such materials because a band is superimposed between higher soil values and lower rock values.

The lower strength limit established by specific classification does not eliminate the difficulty in determining a clear boundary between very soft and hard rocks as well as stiff and cohesive soils because the materials situated in this transition domain can behave as soils or rocks depending on the stress application conditions (Hencher, 1993).

To predict the lateral strength of a piling embedded in rock, the constitutive rupture model must incorporate coupling between lateral friction and normal displacement models in its analyses (Pease & Kulhawy, 1984; Seidel & Haberfield, 1995) as well as facilitate description of the behaviour of lateral strength from initial loads through complete mobilisation, which leads to a rupture. The models require numerical accuracy for parameters that are not typically evaluated in engineering. It is common to use parameters, such as rock cohesion (c), angle of friction (j) and uniaxial compressive strength (q_u), that are generated through Equation 1 and Table 1 (Horvath et al., 1980; Williams & Pells, 1981; Amir, 1986; Rowe & Armitage, 1987; Kulhawy & Phoon, 1993).

$$q_{ult} = q_u = 2 \cdot c \cdot \tan(45° + \varphi/2) \quad (1)$$

The stress-strain parameters, Ei, for rocks were taken from the correlations presented by Hoek et al (2002) and also from the resistance to uniaxial compressive strength (q_u).

For the soil and weathered rock surface layers, estimates for strength parameters can be generated through empirical and semi-empirical correlations, which produce estimated values for cohesion, angle of friction and modulus of elasticity as functions of depth, as shown in Equations 2, 3, 4 and 5.

$$\varphi = 28° + 0.4 \cdot N_{SPT} \text{ (Godoy, 1983)} \quad (2)$$

$$\varphi = \sqrt{20 \cdot N_{SPT}} + 15° \text{ (Teixeira, 1996)} \quad (3)$$

$$c_u = 10 \cdot N_{SPT} \text{ (kPa) (Teixeira \& Godoy, 1996)} \quad (4)$$

$$E_i = K \cdot N_{SPT} \cdot 3.4 + 130 \text{ (where K = 3.5) (kgf/cm}^2\text{) (Trofimenkov, 1974)} \quad (5)$$

RQD (%)	Rock property		
	Uniaxial resistant strain	Cohesion (c)	Angle of friction (j)
0 – 70	0.33	0.10	30°
70 – 100	(0.33-0.80)	0.10	30°- 60°

Table 1
Reduction of force parameters for a rock mass (Kulhawy & Goodman, 1987).

2. Estimation of geotechnical parameters

To estimate the geotechnical parameters for the local subsoil, various sounding experiments were performed and are shown in Figure 1; the average depth value is shown in Figure 2. Based on these experiments, it was found that the subsoil is composed of a 3 to 5 m thick surface layer of moderately stiff clay followed by a 2 to 3 m thick weathered rock layer. A substrate that was limiting for the sounding experiments is found after the second layer and is composed of basaltic rock with above-average fracturing and regular to good recuperation with RQD values between 70 and 90% depending on the sounding location.

The sounding profiles shown have a coefficient of variation (CV) with N_{SPT} values as a function of depth (Figure 2), wherein elevated variability is shown between 5 and 7 m deep. An abrupt increase in the N_{SPT} values was also observed 5 m deep; further, the soundings were limited by a percussion advance

through 8 m deep. The average N_{SPT} values shown in Figure 2 were used as base parameters to generate the soil mechanical characteristics necessary for numerical analyses (Figures 3, 4 and 5). For the rocky massif, the correlations in Equation 1 and Table 1 were used. However, the data in Table 2 were used as a guide.

From the cohesion values, an essential parameter was generated for use in the numerical analyses, the adhesion factor (α). This parameter facilitates the characterisation of an element for the interface between the foundation element and its surroundings (soil and rock). Therefore, the graph in Figure 6 proposed by Tomlinson (1957) was used.

The values of the geotechnical parameters for the different layers that comprise the subsoil are shown in Table 2. The estimates related to the rocky massif geotechnical properties were generated in accordance with Bieniawski (1989). However, a greater or lesser value is attributed to the respective parameters for the rock as a function of its RQD.

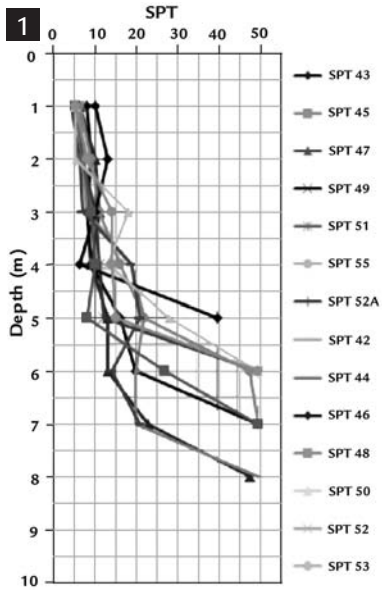

Figure 1
Profile I of SPT sounding.

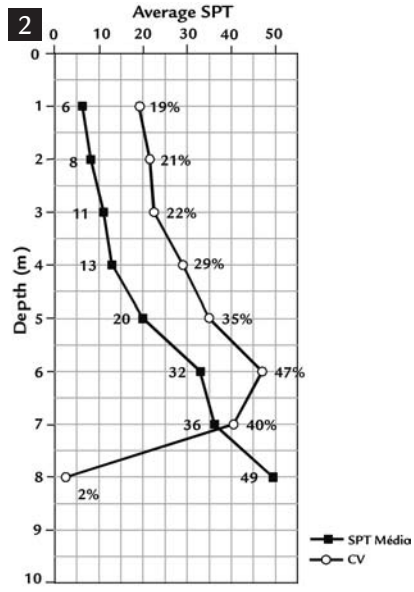

Figure 2
Average N_{SPT} values.

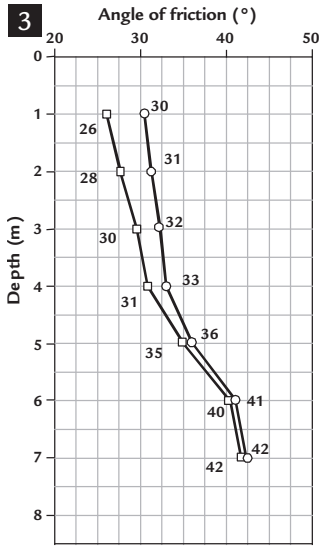

Figure 3
Angle of friction variation as a function of depth.

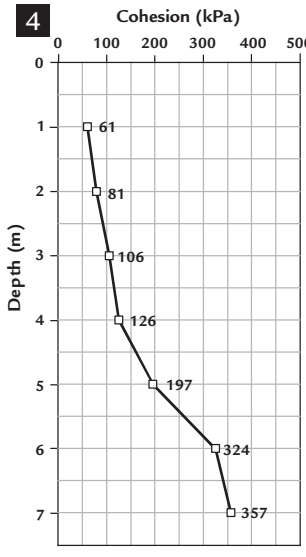

Figure 4
Cohesion variation as a function of depth.

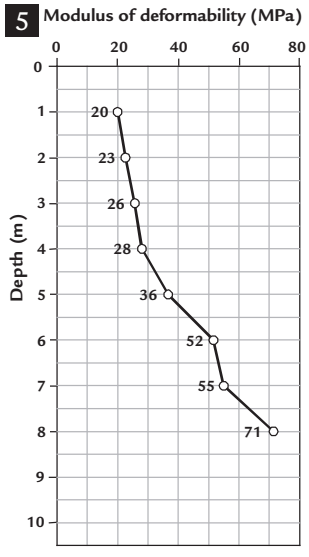

Figure 5
Modulus of deformability variation as a function of depth.

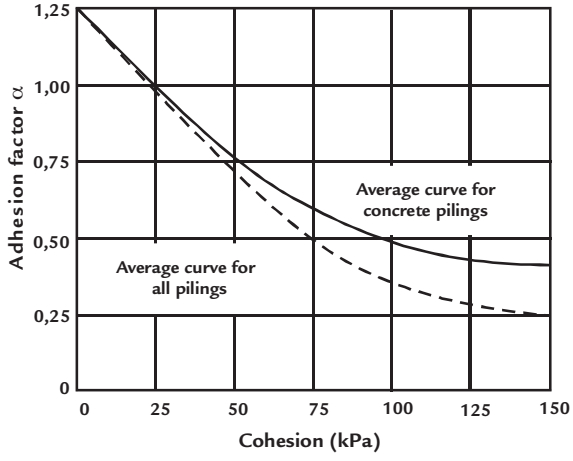

Figure 6
Adhesion factor α (Tomlinson, 1957).

Material	γ	c	φ	ν	α	E_i
Clay	1.80	40	27	0.33	0.75	10-40
Weathered rock	2.00	50-150	30-40	0.20	0.70-0.25	50-150
Rock (basalt)	2.60	200-400	35-50	0.16	0.25	10,000-70,000

γ - Specific weight (kN/m³); c - cohesion (kPa); φ - Angle of friction (°); ν - Poisson Coefficient; α - adhesion factor; and E_i - Modulus of elasticity (MPa).

Table 2
Parameters adopted for each material use in numerical modelling.

3. Foundation pilings

The foundation pilings (nominal diameter = 0.41 m) were constructed in accordance with the NBR6122/10 and ABEF manual (2006) guidelines.

In Table 3, the final length of each piling is presented with the respective embedding length for each layer (soils, weathered rock and bedrock).

Block	Piling	Embedding length by layer (m)			
		Soil	**Altered rock**	**Bedrock**	**Total (m)**
B21	18	3.0	ND	6.0	9.0
B41	15	7.0	4.0	11.0	22.0
B56	13	5.5	7.0	8.5	21.0
B55	07	7.0	5.5	ND	12.5

ND: not detected.

Table 3
Composition for the piling lengths in the mass.

4. Load tests

Four slow maintained load (SML) tests were performed in accordance with the ABNT NBR12131/2006 guidelines (i.e., the loads were performed in equal and successive stages at no greater than 20% of the expected working load for each piling tested). The aforementioned load tests were performed where the new campus for the Federal University of Latin-American Integration (Universidade Federal da Integração Latino-Americana – UNILA) is under construction. To minimise variations in the massif properties and limitations, the load tests were performed during August 2012.

5. Numerical modelling

Modelling was performed based on ¼ of the problem in question given the symmetry along the piling axis, and thus, 10 m x 10 m rectangular section blocks were generated with variable depths as a function of the length of the analysed piling, including at least 10 m below the piling point. The dimensions used were determined based on the tests performed to ensure that the surrounding conditions used at the ends of the problem can be considered immovable or that they have small displacements; consequently, the dimensions cannot influence the results. An elasto-plastic model was used, which varies as a function of the applied stress following a non-linear model. The finite element mesh was composed of triangular elements with quadratic interpolation that were extruded at each meter of depth.

The properties attributed to each different layer of soil and rock follow the Mohr-Coulomb criteria (i.e., the values for the specific weight (γ), cohesion (c), angle of friction (ϕ), modulus of deformation (E) and Poisson coefficient (ν) were inserted). For the materials with fragile behaviour (Parabolic Model), such as the concrete and mortar, values for compressive strength, traction (Rt), specific weight, modulus of deformation and Poisson coefficient were used.

The CESAR v.5 software from Itechsoft was employed in the analyses, which facilitated the use of a contact element that facilitated the definition of specific properties at the threshold between materials with distinct behaviours or properties that were altered by the execution process. In this case, the specific properties E, c, ϕ and Rt were used in the analyses.

6. Results

Next, the experimental results generated by performance of the four load tests and finite element numerical analyses are presented. Figures 7, 8, 9 and 10 show the load test results for each piling and graphs that compare the results from the experiments and numerical simulations using the software. The numerical analyses comprised tests for a 3000 kN load employed in the field (maximum load for the load test), and the respective loading stages were observed.

From Figure 7, a geotechnical rupture is observed in piling 7, which showed settling greater than 50 mm with the working load (1500 kN) equal to 4.13 mm. In the same figure, the numerical analysis using FEM-3D indicates a geotechnical rupture and settling for the 1500 kN load ($Q_{working}$) at 6.79 mm.

The curves shown in Figures 8 (piling 15), 9 (piling 18) and 10 (piling 13) did not characterise a geotechnical rupture given the low displacement values

produced by the maximum load (3000 kN). However, these figures indicate that the settling values demonstrated using FEM-3D were 1.15, 1.93 and 1.32 mm compared with the experimental settling values produced by the load tests at 0.96, 1.90 and 1.37 mm, respectively, for pilings 15, 18 and 13.

The settling values from the load test and numerical analyses for the working load (1500 kN) are shown in Table 4.

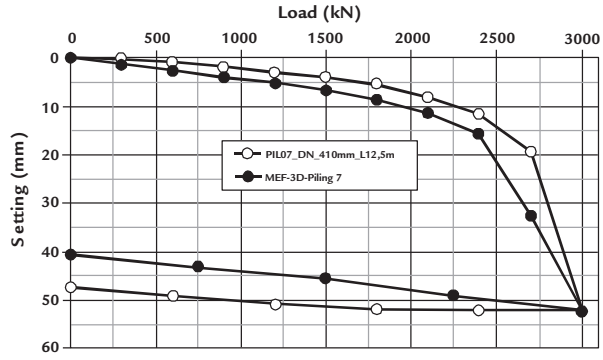

Figure 7
Load-settling curve from the load test and FEM-3D numerical analysis for piling 07.

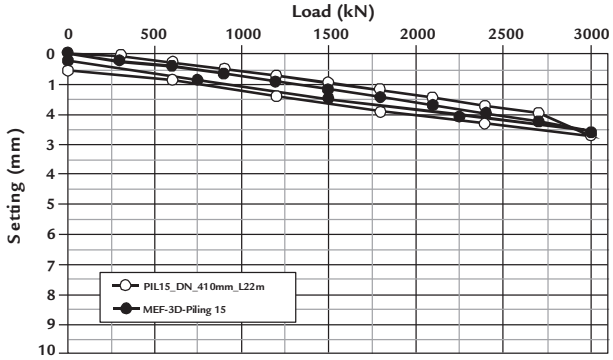

Figure 8
Load-settling curve from the load test and FEM-3D numerical analysis for piling 15.

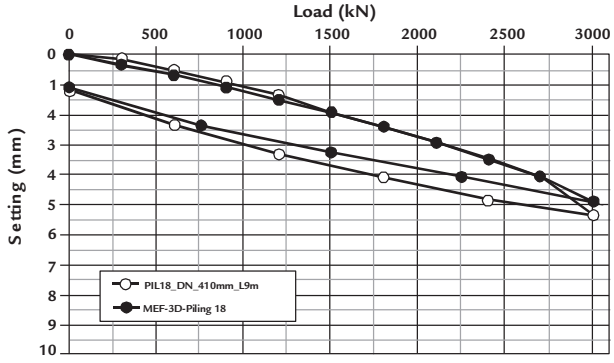

Figure 9
Load-settling curve from the load test and FEM-3D numerical analysis for piling 18.

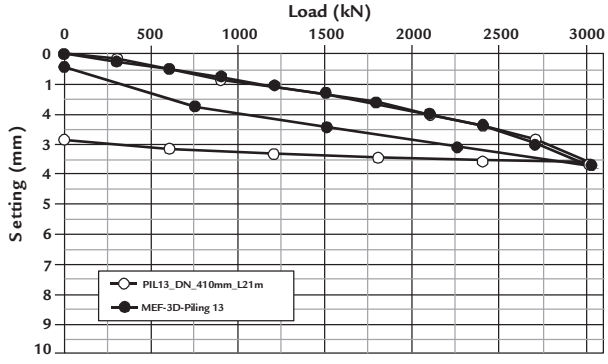

Figure 10
Comparison between the load-settling curve and FEM-3D numerical analysis for piling 13.

Piling	L/ϕ	LT (mm)	FEM-3D (mm)
No. 15	54	0.96	1.15
No. 13	51	1.37	1.32
No. 07	30	4.13	6.79
No. 18	22	1.90	1.93

Table 4
Settling values generated by the load tests and numerical modelling for the 1500 kN load.

LT: Load Test; FEM-3D: Three-dimensional Finite Element Method.

The settling values for the working load are compared in Figure 11, which shows the L/ϕ relationships equal to 22 (piling 18), 30 (piling 7), 51 (piling 13) and 54 (piling 15). The numerical model showed variation ranging from 1.5%, 64.4%, -3.6% and 19.3%, respectively. According to Figure 12, the settling behaviour as a function of variation in the relationship with rock embedding (Lr/ϕ) is shown. Notably, when the Lr/ϕ relationship increases, the settling tends to decrease.

The numerical analyses verified the enhanced impact of the pilings embedded in layers of material with different rigidity values (E) on the load distribution behaviours at different depths, as shown in Figures 16, 17, 18 and 19.

Figure 13 shows uniformly low dissipation of lateral friction from the top of piling 15 through approximately 7 m deep in the soil. However, beginning at this depth, the slope increases for the line of load dissipation through its complete exhaustion at 15 m deep in a layer composed of weathered rock and bedrock. Based on this depth, the lateral friction is negligible, and the tip strength was not verified. From Figure 14, it is confirmed that the load distribution along the piling 7 shaft is dissipated through complete exhaustion at the tip region, which contributes only 2% to the final load value (stage 10).

In Figure 15 (piling 13), dissipation by lateral friction was observed through 57% of the total piling length; it was most effective beginning at 5 m deep. It is emphasised that the shaft is embedded in the layer of weathered rock and bedrock in this region.

Figure 16 shows the behaviour of piling 18, which is the only piling not embedded in the material with elevated rigidity (bedrock). In this case, the load distribution as a function of depth demonstrates that it is different from the other pilings. The 16% contribution by the tip is shown through the maximum load value. Note that the section of piles no. 13 and 15 that is driven in bedrock provides little lateral friction resistance, since the load was previously dissipated in the upper layers composed of soil and modified rock. This demonstrates that the length of these piles could have been reduced.

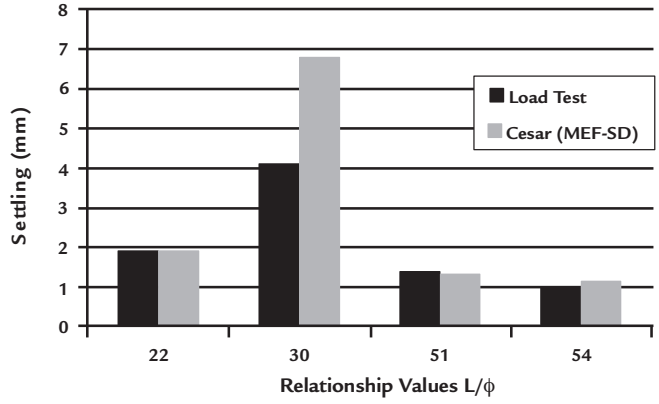

Figure 11
Variation between the settling value from the load tests and numerical simulations.

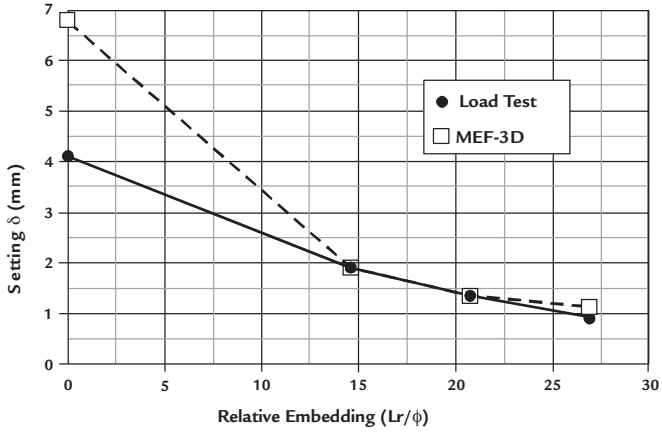

Figure 12
Rock embedding (Lr) variation as a function of settling.

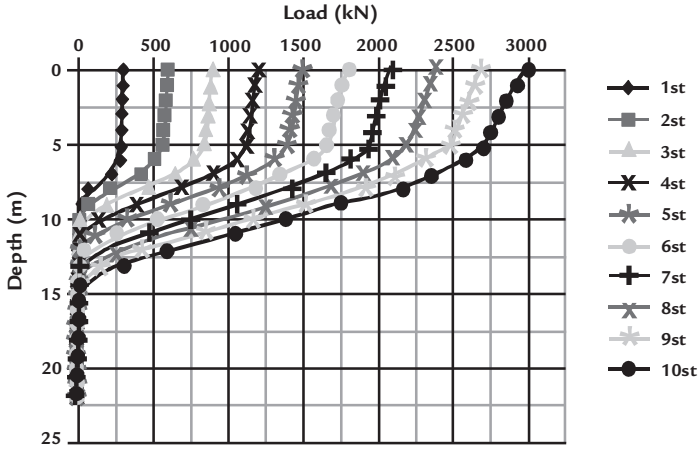

Figure 13
Load transfer as a function of depth for piling 15 (L=22 m).

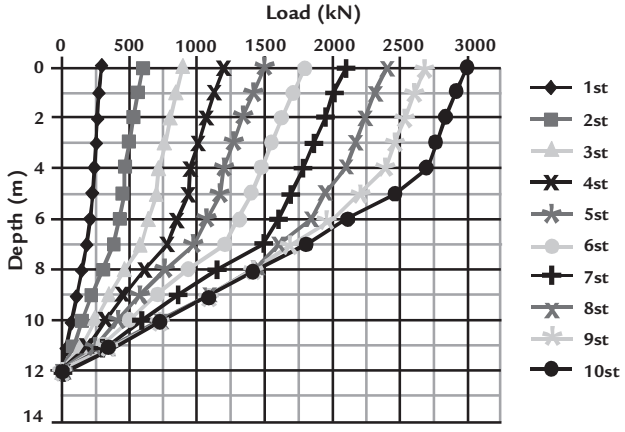

Figure 14
Load transfer as a function of depth for piling 7 (L=12.5 m).

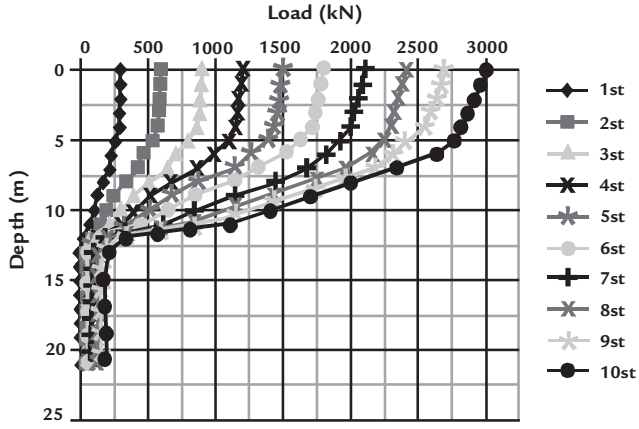

Figure 15
Load transfer as a function of depth for piling 13 (L=21 m).

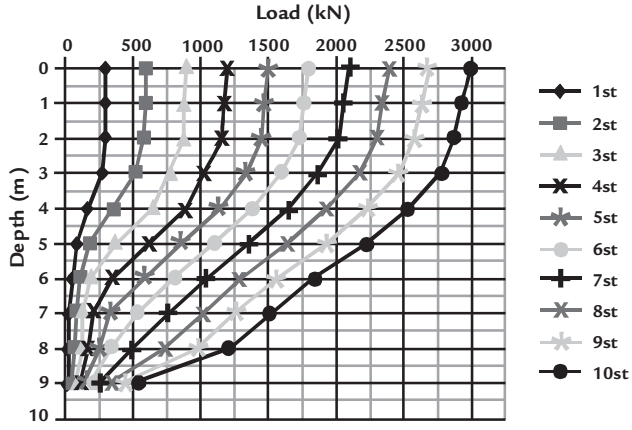

Figure 16
Load transfer as a function of depth for piling 18 (L=9 m).

The distribution of lateral friction for the working and maximum loads is shown in Figures 17 to 20.

The analyses show that a large portion of the lateral friction was absorbed in the weathered rock layer (07, 13 and 15), which generated friction values greater than 270 kPa. For these pilings, a small contribution of the portion embedded in rock is noted. Piling 18 showed a different behaviour; notably, there is no weathered rock, including in the tip load.

7. Conclusions

The tests performed and numerical analyses employed provide sufficient information to discern the behaviour of foundation pilings in rock. Notably, delimitation of the layers that comprise the subsoil must be evaluated geologically using the shear strength parameter values.

The predicted numerical model for the load-settling curve was satisfactory, even for the pilings embedded in materials with an elevated modulus of rigidity and compressive strength. The geotechnical parameter estimates from the formulas based on the field tests facilitated determination of the behaviour for the load-settling curve with good precision through the numerical model.

Distribution of the load as a function of depth generated using the numerical analyses was significantly affected by the portion of the shaft embedded in high-rigidity materials (bedrock) because its dissipation depends on cohesion (c) and rigidity (E).

The portion of the tip strength is approximately zero for the pilings in materials with rock characteristics (i.e., high rigidity). The settlings measured using the load tests and numerical modelling were directly influenced by embedding in rock. The rocky substrate has more influence as a support element for the upper layers and induces more absorbance of the applied load.

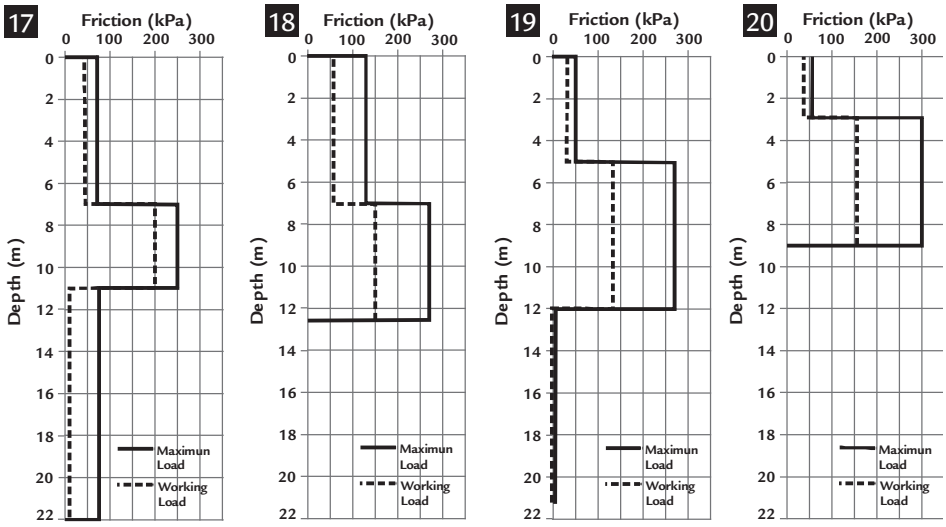

Figure 17
Distribution of friction for piling 15.

Figure 18
Distribution of friction for piling 7.

Figure 19
Distribution of friction for piling 13.

Figure 20
Distribution of friction for piling 18.

8. Acknowledgments

The authors thank the engineers Rogério José Magalhães Pires and Marco Aurélio de Oliveira from the Mendes Júnior Trading and Engenharia S/A company for the data provided in preparation of this article.

9. Bibliographic references

AMIR, J. M. ***Piling in Rock***. Rotterdam: Balkema, 1986. 112p.

ASSOCIAÇÃO BRASILEIRA DE ENGENHARIA DE FUNDAÇÕES [BRAZILIAN ASSOCIATION OF ENGINEERING OF FOUNDATIONS]. ***Research on Foundation Engineering***. São Paulo: ABEF/USP, 2006. 410p.

BIENIAWSKI, Z.T. ***Engineering rock mass classifications***. New York: Wiley, 1989. 249p.

GODOY, N. S. ***Fundações [Foundations]***. Engineering School of São Carlos - USP, 1972. (Class Notes, Undergraduate Course).

GODOY, N. S. ***Estimativa da capacidade de carga de estacas a partir de resultados de penetrômetro estático. (Estimate of the load capacity of pilings from the results of a static penetrometer)***. Lecture given at the Engineering School of São Carlos – USP. 1983.

HENCHER, S. R. Conference summary. The Engineering Geology of Weak Rock. In: ANNUAL CONFERENCE OF THE ENGINEERING GROUP OF THE GEOLOGICAL SOCIETY, 26. ***Proceedings…*** Leeds, United Kingdom: 1993. p. 499-504.

HOEK, E., CARRANZA-TORRES, C., CORKUM, B. Hoek-Brown failure criterion - 2002 Edition. In: NORTH AMERICAN ROCK MECHANICS SYMPOSIUM, 5. ***Proceedings…*** Toronto, July 2002, p. 267-273.

HORVATH, R. G., KENNEY, T. C., TROW, W. P. Results of tests to determine shaft resistance of rock socketed drilled piers. In: INTERNATIONAL CONFERENCE ON STRUCTURAL FOUNDATIONS ON ROCK, ***Proceedings…*** Sidney, 1, p. 349-361, 1980.

KULHAWY, F. H., PHOON, K. K. ***Drilled Shaft Side Resistance in Clay Soil to Rock, Design and Performance of Deep Foundations***, ASCE STP, v. 38, p. 172-183. 1993.

KULHAWY, F. H., GOODMAN, R. E. ***Foundation in Rock, Ground Engineering References Book***. F. G. BELL (ed.), Butterworth, London, 55/1-55/13. 1987

SEIDEL, J. P., HABERFIELD, C. M. The axial capacity of pile sockets in rocks and hard soils. ***Ground Engineering***, v. 28, n. 2, p.33-38, 1995.

TEIXEIRA, A. H. Projeto e execução de fundações [Design and execution of foundations]. In: SEMINÁRIO DE ENGENHARIA DE FUNDAÇÕES ESPECIAIS E GEOTECNIA [SEMINAR OF ENGINEERING OF SPECIAL AND GEOTECHNICAL FOUNDATIONS], 3. ***Anais...*** São Paulo, 1996. v.1. p. 33-50.

TEIXEIRA, A. H., GODOY, N. S. Análise, projeto e execução de fundações rasas [Analysis, design and execution of shallow foundations]. In. HACHICH et al. (eds). ***Fundações: teoria e prática [Foundations: theory and practice]***. São Paulo: Pini, 1996. p. 227-264.

TOMLINSON, M. J. The adhesion of piles driven in clay soils. In: INTERNATIONAL CONFERENCE ON SOIL MECHANICS AND FOUNDATIONS ENGINEERING, 4. ***Proceedings…*** London, 1957, v. 2, p. 66-71.

WILLIAMS, A. F., PELLS, P. J. N. Side resistance of rock sockets in sandstone, mudstone and shale, ***Canadian Geotechnical Journal***, 18, p. 502-513, 1981.

TROFIMENKOV, J. G. Penetration Test in URSS - State-of-the-Art-Report. In: EUROPEAN SYMPOSIUM ON PENETRATION TESTING, 1. ***Proceedings…*** Stockholm National Swedish Building Research, 1974. p. 147-154.

Artigo recebido em 01 de março de 2013. Aprovado em 12 de agosto de 2013.